Prospects for studying the effect of electronic screening on α decay in storage rings

F. F. Karpeshin [*]

D. I. Mendeleyev Institute for Metrology, 190005 Saint-Petersburg, Russia

M. B. Trzhaskovskaya [†]

National Research Center "Kurchatov Institute"—Petersburg Nuclear Physics Institute, 188300 Gatchina, Leningradskaya Oblast, Russia

L. F. Vitushkin

D. I. Mendeleyev Institute for Metrology, 190005 Saint-Petersburg, Russia

Study of the role of electron screening in α decay is advanced, aimed at experimental testing in storage rings. To this end, systematic calculation of the effect in heavy ions of the nuclei within the Ra to Po domain of α emitters is conducted using the adiabatic approach. The effect obtained is to slow the decay down by an amount within a percent value. It is of the opposite sign compared to predictions by the conventional frozen shell model. The reason for the divergence is pointed out. Testing this difference experimentally in storage ring facilities is discussed.

I. INTRODUCTION

α decay plays a significant role both in practical applications and scientific research, starting from astrophysics (e.g., Ref. [1]) up to laboratory research in plasma physics. At the same time, there is a contradiction between laboratory study, which considers nuclear reactions with no respect to a possible role of the electron shell or environment, and applications, which deal with various electronic shells or environments. Specifically, α decay affects nuclear synthesis in the stars. Taking into account the screening effect in ultra-high-density stellar environments might become significant and would deserve further investigation. The beginning was laid, for example, in Refs. [2].

Another astrophysical issue is related with the time reversibility of nuclear reactions occurring in interior of stars, whose study is one of the most promising areas of modern nuclear physics. Most of these reactions encounter similar problems, as the α decay, aggravated by extremely small cross sections at small energies, is still not available for direct measurements in the laboratory. Consequently, indirect approaches are developed in order to better know their cross sections and rates, such as the asymptotic normalization coefficients or the Trojan horse method (e.g., Ref. [3]). From this viewpoint, direct information on the rates and role of electron screening in the reverse process of α decay becomes important.

Surprisingly, up to Ref. [4] in 2013, everybody considered this question within the framework of the frozen electron shell (FS) model (e.g., Refs. [5–9] and references cited therein), although electrons are four orders of magnitude lighter than the α particles and are certainly strongly affected by the α particle slowly traversing the shell. The calculated results were of different signs, in contrast with simple arguments, which can be readily shown based on the physical ground [10]. One of them is a well-studied, both experimentally and theoretically, suppression of prompt fission in muonic atoms of actinides. We discuss this case in Sec. III. The arguments suggest that the electron environment *retards* the decay. This might promote formation of heavy elements and actinides in the r process in the stars.

When considering usual, electronic atoms, one has to involve interaction of the α particle with the electronic shell. The main difficulty which arises in this way is interplay of the two different scales involved. From one side, there is a decrease of $\Delta B \approx 40$ keV in the energy of α particles. This arises and is finally formed on distances of the atomic scale. It is expected to act as to suppress the decay [5]. In contrast, from the other side, α decay is predetermined by the strong short-range α-nucleus interaction. Its influence is ruled out on the outer turning point of the Coulomb barrier, which is essentially inside the electron shell, being tens of Fermi from the nuclear surface. As a result, an intuitive expectation is that the shell should not affect the probability significantly. Moreover, in this region the electrons produce a negative potential for the α particle, which may be assumed to facilitate the decay. A consecutive account of all these factors only can be performed within the adiabatic approach [4]. An analogy was noted with suppression of prompt fission in muonic atoms of actinides. That example teaches that it is not the electronic potential that is so important but its gradient, determining the force acting on the α particle. Important experimental research details

———————
[*]fkarpeshin@gmail.com
[†]Deceased.

were elaborated in Refs. [10,11]. Furthermore, the adiabatic approach was applied and extended in Refs. [12,13]. Herein, we advance the study of the effect and discuss a feasibility of experimental test for it, using such contemporary facilities like experimental storage rings (ESR), available, e.g., at GSI and IMP Lanzhou. In the next section, we mention the principles of the model. Numerical results for the isotopes of Po to Ra domain are obtained in Sec. IV. Prospects of the experimental study are discussed in Sec. V. A summary is derived in Sec. VI.

II. REMIND OF THE MODEL: PHYSICAL PREMISES

Within the framework of the Gamow theory, a conventional expression for α-decay probability is essentially given by product of the two factors: the probabilities of cluster preformation and its penetration outside through the potential barrier. The former is assumed not to be affected by the shell. The latter factor P is determined by action S as follows:

$$P = e^{-2S} \tag{1}$$

with

$$S = \int_{R_1}^{R_2} \sqrt{2m[E - V(R)]} dR. \tag{2}$$

Here $V(R)$ is the potential energy of interaction of the emitted α particle with the rest of the system, including interaction with the nucleus and the electronic shell in the case of atomic system. m is the mass of the α particle, and E is its kinetic energy in the asymptotic region where $V(R)$ can be neglected. Furthermore, R_1, R_2 are the turning points. The effect of electron screening is then expressed as

$$Y = P_a/P_n - 1, \tag{3}$$

where subscripts n and a indicate either the case of bare nuclei or atoms, respectively. The problem of consistent taking into account the aforementioned factors became a stumbling block for many early calculations. The study of Patyk *et al.* [9], who performed the most consistent calculations of α decay for the chain of radon isotopes, put a period to the development of the FS model.

In more detail, in the case of bare nuclei, the potential energy consists of the strong short-range component $V_n(R)$, the centrifugal repulsion $V_{cf}(R)$, and the Coulomb attraction $V_{Coul}(R)$. It reads as follows:

$$V(R) = V_n(R) + V_{cf}(R) + V_{Coul}(R) \equiv V_N(R). \tag{4}$$

Nuclear potential $V_n(R)$ calculated for ^{226}Ra, with the parameters from Ref. [14], is illustrated in Fig. 1. It looks like a shallow well, formed by superposition of the Coulomb repulsion and the strong potential well $V_n(R)$ in the nuclear vicinity, and a flat wide slope formed by $V_{Coul}(R)$ at more distant R. The straight line shows the energy of the emitted α particle. The centrifugal potential $V_{cf}(R)$ arises in the case of the angular momentum of the α particle $L \neq 0$ and is not shown in the figure. It only slightly modifies the shape of the barrier, somewhat changing the effect of the electron shell in the third decimal.
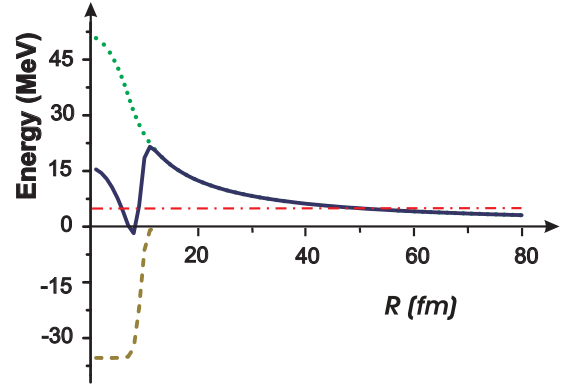
FIG. 1. Potential energy of the α particle interaction with the nucleus (thick full curve), resulting from the superposition of the strong attractive potential well (dashed curve) and the repulsive Coulomb interaction (dotted line).

In atoms, the potential energy of the adiabatic $e - \alpha$ interaction of the α particle with the electronic shell $U_{e-\alpha}^{ad}(r)$ is added:

$$V(R) \equiv V_a(R) = V_N(R) + U_{e-\alpha}^{ad}(R). \tag{5}$$

Furthermore, the Q value is changed by ΔQ because of the rearrangement of the shell in the daughter atoms, with the related change of the total electron binding energy $\Delta B \equiv -\Delta Q$. The resulting expression for the action integral becomes as follows:

$$S_a = \int_{R_1'}^{R_2'} \sqrt{2m[E - V_N(R) + \Delta Q - U_{e-\alpha}^{ad}(R)]} dR. \tag{6}$$

In order to better realize the difference between the adiabatic and FS models, let us dwell in more detail than was done in Refs. [4,10] on the construction of the prompt adiabatic potential of the $e - \alpha$ interaction $U_{e-\alpha}^{ad}(R)$. It is one of the main constituents of the adiabatic method. Let us put down a general expression as follows:

$$U_{e-\alpha}^{ad}(R) = -\zeta e^2 \int \frac{\rho_e(r)}{|\mathbf{r} - \mathbf{R}|} d^3r + \text{const}, \tag{7}$$

with $\rho_e(r)$ being the prompt electron density, and $\zeta = 2$ being charge of the α particle. $\rho_e(r)$ depends on R. It can be considered as spherically symmetric at $R < R_s$, R_s being the point of appearance of the α particle on the nuclear surface. Its value is usually calculated by means of the self-consistent method (e.g., Ref. [15]),

$$\rho_e(r) = 4\pi \sum_i N_i [G_i^2(r) + F_i^2(r)], \tag{8}$$

where $G_i(r)$ and $F_i(r)$ are the radial Dirac electron wave functions, normalized as follows:

$$\int_0^\infty [G_i^2(r) + F_i^2(r)] dr = 1. \tag{9}$$

Summation in Eq. (8) is performed over the shells i, with N_i being the occupation numbers. We introduced an arbitrary constant in Eq. (7), which we define later. By definition, the e-α interaction potential in the FS model is obtained with

const $= 0$. Starting from this moment, at $R > R_s$, $G_i(r)$ and $F_i(r)$ depend on R. This is an important element constituting difference between the FS model and the adiabatic approximation. Increasing R also increases the rms radius of the total nuclear charge, which diminishes the binding energy of the atom and increases the electronic term [4,10]. Furthermore, the electronic density gradually becomes aspherical, following the motion of the α particle. For the calculation, in the first order of the perturbation theory this effect can be neglected at small R around the nuclear surface, including a physically interesting subbarrier region. Then Eq. (7) can be expressed as follows:

$$U_{e-\alpha}^{\text{ad}}(R) = 4\pi\phi(R) + \text{const}, \tag{10}$$

$$\phi(R) = u(R) - \frac{\zeta z e^2}{R_e}, $$

$$u(R) = -\zeta e^2 \sum_i N_i \int_0^R \left[G_i(r)^2 + F_i^2(r)\right]\left(\frac{1}{R} - \frac{1}{r}\right)dr, \tag{11}$$

$$\frac{1}{R_e} = \sum_i N_i \int_0^\infty \left[G_i^2(r) + F_i^2(r)\right]\frac{dr}{r}. \tag{12}$$

Here we denoted z as the number of electrons in the atom, not to be mixed with the atomic number Z. By definition, the function $\phi(R)$ determines the potential in the FS model. We normalize the constant by the natural boundary condition:

$$U_{e-\alpha}^{\text{ad}}(R) \to 0 \quad \text{at} \quad R \to \infty. \tag{13}$$

One cannot apply condition (13) to the expression (10) yet, in view of that expansion (11) is not valid at large R.

Note that at the starting point, the potential energy of e-α interaction is $U_{e-\alpha}^{\text{ad}}(R_s)$. Then, according to the Feynman-Hellman theorem [16], within the framework of the adiabatic approach, the work $w(R)$ done by the α particles over the electron shell when moving from the starting point R_s to a point R acquires a usual form depending on the potential difference at the end and start points:

$$w(R) = \int_{R_s}^R \frac{dU_{e-\alpha}^{\text{ad}}(R')}{dR'} dR' = U_{e-\alpha}^{\text{ad}}(R) - U_{e-\alpha}^{\text{ad}}(R_s). \tag{14}$$

The constant which is not defined yet cancels out in Eq. (14). This equation with the account of (13) allows one to express the constant in terms of ΔQ. Going to the limit $R \to \infty$, one obtains that

$$\Delta Q = U_{e-\alpha}^{\text{ad}}(R_s). \tag{15}$$

Now condition (15) defines the constant:

$$\text{const} = \Delta Q - \phi(R_s). \tag{16}$$

Substituting Eq. (16) into (6), we see that the effect of the electron shell can be reduced to a mere addition of a purely electronic effective potential [4]

$$W_{\text{eff}}^{\text{ad}}(R) = 4\pi[\phi(R) - \phi(R_s)]$$

$$= -4\pi\zeta e^2 \sum_i N_i \int_{R_s}^R \left[G_i(r)^2 + F_i^2(r)\right]\left(\frac{1}{R} - \frac{1}{r}\right)dr \tag{17}$$
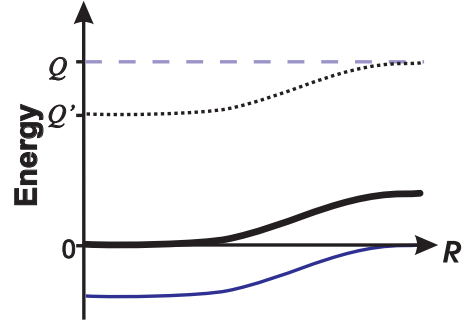
FIG. 2. Scheme of taking into account the electronic contribution to the effective α potential. Thin and thick solid lines indicate adiabatic and effective adiabatic e-α potentials $U_{e-\alpha}^{\text{ad}}(R)$, Eq. (10) with (16), and $W_{\text{eff}}^{\text{ad}}(R)$ (17), respectively. Q and Q' are the energies released in the case of α decay either of bare nuclei or the neutral atoms, respectively. They differ just by the growth of $W_e(R)$. The atomic calculations should be performed, using Q' and $U_{e-\alpha}^{\text{ad}}(R)$, but the results hold if Q and $W_{\text{eff}}^{\text{ad}}(R)$ are used instead of them, respectively.

inside the integral in Eq. (2). Equation (17) differs from Eq. (11) by the low bound of integration. The energy E in Eq. (2) remains the same as in for bare nuclei. This result is illustrated in Fig. 2. Involving the effective electronic potential $W_{\text{eff}}^{\text{ad}}(R)$ resolves the conflict of scales mentioned in the introduction. It appears as a perturbative positive definite extra potential, reasonably weak enough, which slightly affects the barrier penetration probability. Below, we will mean potential (17) under the α-electron interaction.

The Feynman-Hellman theorem is not relevant in the FS model, because it is only valid for stable systems [16], which obviously do not include a FS model. In this case, one can calculate the e-α interaction potential directly by means of Eqs. (10) to (12) with const $= 0$, while holding the ΔQ value in Eq. (6). In order to compare models, let us also introduce the effective potential for the FS model $W_{\text{eff}}^{\text{FS}}(R)$ by mere inclusion of ΔQ value in $\phi(R)$:

$$W_{\text{eff}}^{\text{FS}} = 4\pi\phi(R) - \Delta Q. \tag{18}$$

Then in both models, the expression for the action integral reads as follows:

$$S_a = \int_{R_1'}^{R_2'} \sqrt{2m[E - V_n(R) - V_{\text{Coul}}(R) - W_{\text{eff}}(R)]}\, dR, \tag{19}$$

with $W_{\text{eff}}(R)$ given by either (17) or (18).

In Fig. 3, the resulting interaction potential of the α particle with the electron shell is presented in more detail in the case of neutral $_{88}^{226}$Ra atoms α decay. The calculations are performed by means of Eqs. (10) to (12), using the RAINE package of computer codes [17]. Figure 3(a) shows a general view of the calculated potentials. At small R, the adiabatic potential starts from $U_{e-\alpha}^{\text{ad}}(R_s) = \Delta Q$ at $R = R_s$. The ΔQ value is calculated as the difference of the total binding energies of the mother and daughter atoms. At large R, qualitative view of the curve is shown. It vanishes at large R as $-\zeta z e^2/R$ in the main term. At small distances, calculation shows that the adiabatic potential turns out to be confined between the FS potentials of the
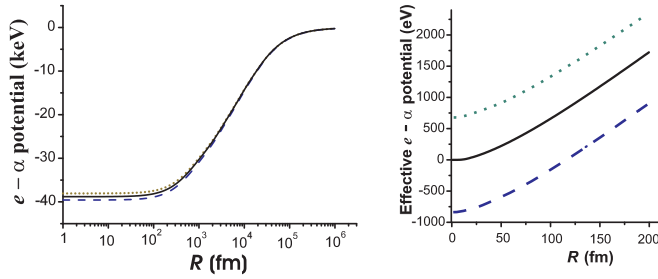
FIG. 3. (a, left) e-α interaction potential energies in the case of decay of neutral ^{226}Ra atoms: the adiabatic approach (full curve), in comparison with the FS potentials in the initial (dashed curve) and final (dotted curve) atoms, respectively; (b, right) the same cases, effective potential energies in the nuclear region.

FIG. 4. Contributions of separate shells into the e-α adiabatic potential in the case of neutral Ra atoms. (a, left) K shell, full curve; L shell, dashed curve; M shell, dash-dotted curve; and N shell, dotted curve. (b, right) The same for He-like ions (dashed curve), Ne-like ions (dash-dotted curve), and neutral atoms (full curve).

atoms Z and $Z - 2$. This is reasonable since the real electronic density evolves from the parent to the daughter atoms.

Figure 3(b) shows the effective potentials in the subbarrier region. The effective adiabatic potential starts from zero value. The effective FS potentials start from the negative and positive values in the initial and final atoms, respectively. Numerically, in the case of ^{226}Ra, $U_{e\text{-}\alpha}^{\text{FS}}(0) = -39.572$ keV was obtained, and $\Delta B = -38.805$ keV. Thus, the FS curve starts from -0.767 keV at $R = 0$. This is in a close agreement with Ref. [9], from where a value of about 750 eV can be concluded (cf. Fig. 1 of Ref. [9]). According to Ref. [18], $\Delta B = 640927 - 679616 = -38789$ eV, which is only 16 eV less than our value. The left and right barrier turning points are $R_1 = 9$ fm, $R_2 = 51$ fm. The three conclusions drawn below clearly follow from Fig. 3:

(i) The effect of the shell on the α decay rate is negative (as the adiabatic effective potential is represented by a positive definite curve).

(ii) In contrast, within the framework of the FS model, the effect is positive (as the corresponding lowest curve really lies below zero in the subbarrier area).

(iii) In the subbarrier region, the absolute value of the adiabatic potential is considerably less than that of the FS model. This explains why the effect within the consecutive adiabatic approach turns out not only to be of the opposite sign, but also considerably less in absolute value.

Moreover, the adiabatic approach allows one to consistently calculate the contribution of each electron shell to the overall effect. This is performed directly by means of Eq. (17). Results are presented in Fig. 4. It follows from Fig. 4 that about 80% of the total screening potential is expected to be due to the contribution from the K-shell electrons. This gives an opportunity of performing an accurate experiment, which we will discuss in Sec. IV. But first, it is time to dwell on the effect of augmentation of the fission barrier in muonic atoms.

III. AUGMENTATION OF THE BARRIER IN FISSION OF MUONIC ^{238}U

The process of prompt fission of actinide nuclei in muonic atoms was predicted by Wheeler [19] as a consequence of radiationless transitions in muonic atoms. Muonic beams stop in matter, after which the muons start to be captured into high
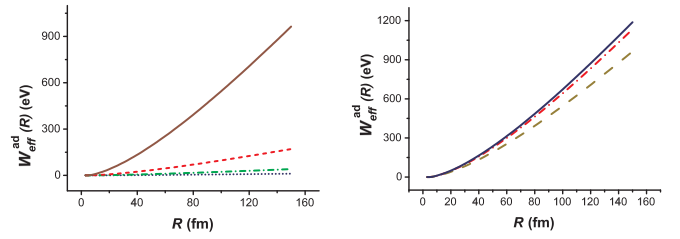
atomic orbits with $n \gtrsim 14$, forming muonic atoms. Then the muons cascade down to the lowest $1s$ orbit, usually by means of radiative or Auger transitions. Wheeler proposed that in the case of ^{238}U, there is a chance of radiationless $2s \rightarrow 1s$ muonic transition. Its energy of about 7.5 MeV is transferred to the nucleus, which can undergo fission. This fission is called prompt, as occurs promptly for a time of the μ atomic cascade, which is within 10^{-13} s. Alternatively, the muon can be captured in the K orbit by the nucleus, also inducing fission. This kind of fission is called delayed fission, as it occurs with the lifetime of the muon in the orbit, which is ≈ 70 ns. These two kinds of fission can be separated electronically. However, the electrical dipole radiative transition $2s \rightarrow 2p$ makes a strong competition to the fission channel, and the probability of population of the $2s$ level is a few percent only. However, Zaretsky pointed out that there is a large probability $\approx 50\%$ of the nuclear excitation in the transitions $2p \rightarrow 1s$ and $3p \rightarrow 1s$ as well [20]. In this case muons survive in the K orbit during the fission process, and then they are entrained on a fragment, usually the heavy one. Hence, the muons appear as spectacles of fission. Their presence in the orbit can be used for study both of the static properties of actinide nuclei and the fission dynamics. They are illustrated in Fig. 5. Measuring the radiationless transition probabilities presents an opportunity
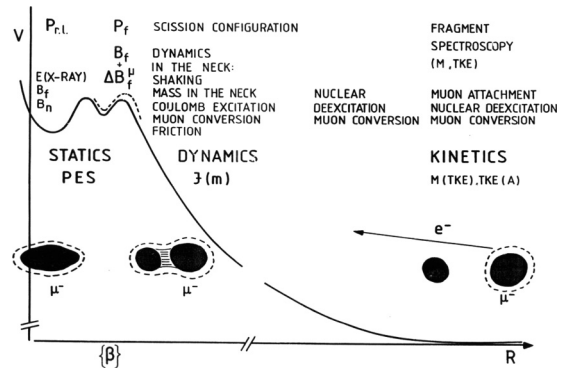
FIG. 5. Directions of research on the static properties of fissile nuclei in the equilibrium state (PES), together with the fission dynamics in muon-induced prompt fission. Study of postfission processes in the fragments provides information on the neutron-rich radioactive nuclei.

to study fine structure of the giant nuclear resonances with monoenergetic virtual photons of pure multipolarity: electric dipole resonance (GDR) in the $2p \rightarrow 1s$ and $3p \rightarrow 1s$ transitions, quadrupole resonance in the $3d \rightarrow 1s$, $4d \rightarrow 1s$, and low-lying octupole resonance in the $3d \rightarrow 2p$ radiationless transitions. The measured probabilities are up to 30% for the majority of these transitions (Ref. [21] and references therein), and 90% in the case of the $3p \rightarrow 1s$ transition, closest to the resonance with the GDR.

Many possibilities are available to study the fission dynamics. First, it is muon distribution of the fragments. The muons usually stick to the heavy fragments. However, there is a small probability of entrainment on the light fragment. The latter essentially depends on viscosity of the nuclear matter, friction on the path toward fission, shape of the neck, and muon shake-off as a result of snapping back the remnants of the neck. The presence of a muon in one or another fragment can be detected due to muon capture in the fragment, muon decay in the orbit into an electron, neutrino, and antineutrino, muonic internal conversion during deexcitation of the fragments, etc. (e.g., Ref. [22] and references therein). Additional information can be inferred from study of the total kinetic energies (TKE) of the fragments.

Increased interest in the search for prompt fission arose after this prediction was confirmed experimentally [23]. The authors compared intensity of the muonic x rays, corresponding to the $2p \rightarrow 1s$ transitions, in uranium and lead ^{208}Pb. It turned out that the relative intensity in the uranium case was suppressed by about one third. As the branching ratio for photofission in uranium in the energy range around 6.5 up to 12 MeV is approximately 1/5, $\approx$0.06 prompt fission events per muonic atom were expected. The results of the first experiments were surprising. Belovitsky *et al.* [24] used photographic emulsions of $\approx$ 200 μm thick, uniformly loaded with acetate uranyl. The plates were irradiated in the synchrocyclotron of the Joint Institute for Nuclear Research by a beam of slow negative muons. Tracks from the fission fragments were clearly seen at the magnification of 300–2000×. A total of 738 fission events was found. As a result, the probability of uranium fission by muons was found to be 0.070 ± 0.008 per atom. Surprisingly, all of these events turned out to be delayed fissions. There are several ways to distinguish these kinds of fission: Were the fissions observed due to nonradiative transitions, then the emission of heavy (p, α) charged particles from the end of the fragment track would be observed in approximately ten cases, and in eight cases electrons from μ-e decay would be observed. Not a single event of this kind has been observed. Similarly, no conversion muons have been observed, though approximately ten such events were expected. An upper bound was derived for its probability $P_p \lesssim 0.01$ per atom. Such a suppression of fission channel was explained by augmentation of the fission barrier in the presence of a muon in the K orbit.

In more detail, the muonic K orbit goes deeply inside the nuclear surface in the actinide nuclei. Therefore, the presence of the muon in the first approximation can be considered as diminishing the total charge, which should increase the barrier. The muon works like a glue which keeps the fragments together. This explanation was fairly confirmed by the

calculations [25]. The calculations showed that the deformed ellipsoid has up to 1 MeV larger Coulomb energy, which manifests itself as an augmentation of the fission barrier. This decreases the fission probability by an order of magnitude. In absence of the muon, the fission barrier (5.8 MeV in ^{238}U) is a little below the energy of the $2p \rightarrow 1s$ transition. As a consequence, such an augmentation of the barrier changes the fission probability so drastically.

Later on, the Schrödinger equation was solved numerically for a set of deformations of the fissile nucleus [26]. The muonic binding energies, renormalized to zero at the ground-state deformations, showed the augmentation of the fission barrier on the way toward fission. The renormalization is identical to Eq. (15). Thus, the effect of the barrier augmentation was calculated within the framework of the adiabatic approximation. The result was obtained that the muon binding energies monotonically decrease with deformation. Therefore, the more deformation, the stronger the augmentation of the barrier. This predetermines monotonical increase of the fission barrier along the path toward fission. Moreover, in view of the double-humped shape of the fission barrier, a significant stabilizing effect was predicted for the muonic ^{236}U in the isomeric state [26] due to a higher augmentation of the outer barrier. The search for the fission isomers in muonic atoms was undertaken by several authors. Regretfully, it gave no certain evidence.

Subsequent experiments confirmed the theoretical conclusions. In Ref. [27], the absolute fission yield was measured (see also references indicated therein): $P_t = 0.068 \pm 0.013$. Moreover, the prompt-to-delayed fission ratio was obtained as follows: $P_p/P_d = 0.099 \pm 0.005$, from where the prompt and delayed fission probabilities can be extracted as following: $P_d = 0.062$ and $P_p = 0.006$ per muonic atom. These numbers are in excellent agreement with Ref. [24].

It can be concluded from the above probabilities that delayed fission of ^{238}U is also suppressed in comparison with neutron- or photo-induced fission. This is because not ^{238}U, but ^{238}Pa or ^{237}Pa, whose fissibility is much lower, undergo fission as a result of muon capture. Only the prompt fission remains suppressed by the barrier augmentation.

IV. RESULTS

Representative calculations were performed in Refs. [4,10,11] for various α emitters throughout the periodic table and with different decay energies. They show that the effect of screening strongly decreases with increasing Q value and decreasing lifetime. Within the adiabatic approximation, it is evident that the inner electrons produce more effect, as they are more sensitive to the motion of the α particle in the subbarrier area near the nucleus. According to Fig. 4, more than 80% of the effect are produced by the K electrons. This suggests an elegant and basic way of experimental check, e.g., through measurement of the difference in the decay rate between the He-like and bare ions of the same nuclei—α emitters. Monochromaticity parameters of the storage ring beam are good enough in order to detect the recoil nuclei by the Schottky method [28].

TABLE I. Effect of electron screening Y as calculated for different electronic configurations of the ^{226}Ra atom.

Nuclide	Q (MeV)	Neutral	K shell	K and L shells	He-like ion	Ne-like ion
^{226}Ra	4.87063	−0.246	−0.200	−0.235	−0.201	−0.236
^{212}Rn	6.385	−0.086	−0.070	−0.081	−0.071	−0.082

Consider dependence of the decay rate on stripping the electron shell in more detail. Results of calculation for ^{226}Ra and ^{212}Rn atoms are presented in Table I.

The Q values (column 2) are cited according to Ref. [29]. In column 3, the Y values (3), calculated within the adiabatic approach, are presented for the neutral atoms. The partial contributions from the K shells and both the K and L shells, respectively, are listed in columns 4 and 5. In the sixth and seventh columns, the results are listed for the He-like and Ne-like ions, respectively. It follows from these results that 82% of the effect are due to the contribution of the K-shell electrons. Nearly full effect (98%) is achieved in the case of Ne-like atoms. Note that in the case of He-like or Ne-like ions the effect is a little greater than if calculated for neutral atoms with allowance for only the K or both K and L shells, respectively. This fact has a simple explanation on the physical ground. In the ions, the electronic orbitals are more compact around the nuclei, and therefore the wave functions are greater in the area under the Coulomb barrier. This consequently causes bigger values of the integrand in Eq. (17) and the related increase of the effect.

The experiment can be realized in a similar way to which was applied in search for the time modulation in beta decay of Pm ions [30]. The daughter product from the α decay will stay in the ring and should be seen by Schottky analysis. If one starts from ^{212}Rn^{84+}, one should have most of the time ^{208}Po^{82+}, and it will be good to detect both. If one uses bunches of ions then the Schottky needs to be calibrated and one has to find out how well this can be done for the four cases of decay from ^{212}Rn^{84+} and ^{212}Rn^{86+}. The "background" arising from ionization and shake-off from Rn^{84+}, and also possible electron capture by Rn^{86+}, could be made quite weak.

On one hand, the α lifetimes of seconds to minutes seem to be suitable from the viewpoint of experiment using storage rings. On the other hand, the calculated values of Y are mainly determined by the Q values. They weakly depend on the atomic and mass numbers Z, A of the nuclides within the Ra–Po domain. In Fig. 6, we present the Y values as calculated for the isotopes of Ra and Rn against their Q values in neutral atoms. For comparison, results, obtained within the FS model, are also shown in the same figure.

In order to have a big effect, it is desirable to use the isotopes with small Q_α. Small Q_α correlate with long half-lives which may comprise days and years, which is inconvenient for measuring in the storage rings. In Table II, we present the resulting Y values for radium isotopes with half-lives within seconds to minutes and the α branching ratios 100% or close. Most abundant isotope ^{226}Ra and the next ^{222}Ra are characterized with a reasonable effect $Y = -0.25\%$ and -0.14%, respectively, with comparatively long half-lives. Among the lighter isotopes, there are two groups around $A \approx 222$ and 213. They are characterized with the Q_α values of 6–7 MeV

and the effect $|Y| \lesssim 0.1\%$. Results for other such suitable isotopes of Fr, Rn, Ac, At, and Po are listed in Table III.

V. DISCUSSION

Although the predicted magnitude of the effect is as small as about 10^{-3}, there is a circumstance favorable for experimental studies: About 80% of the effect is due to the contribution of the K-shell electrons. In order to observe the effect, it is therefore sufficient to compare the decay half-lives for bare nuclei with the half-lives for respective one- and/or two-electron atoms, without involving neutral atoms; their accumulation in accelerator rings is impossible. Generally, it is more reliable to observe small effects via difference measurements at the same facility. Thus, comparative measurements can be performed in the same storage rings with bare nuclei and respective ions with various degrees of ionization—for example, helium-like or neon-like ions.

An experiment on comparison of the α-decay half-lives in neutral atoms and their H-like ions was already tested at GSI a few years ago [31]. For this purpose, ^{213}Fr and ^{214}Ra nuclei were selected as candidates. They were produced in flight at the Fragment Separator (FRS) of GSI via 1 GeV/u ^{238}U fragmentation with a Be target. However, the measurements with neutral atoms of ^{213}Fr and H-like ions of ^{213}Fr were carried out with different methods. For the neutral lifetime measurements, the ions were implanted in the stopper, consisted of two layers of double-sided Si-strip detectors. As a result, half-lives of 34.0(3) and 2.435(20) s have been extracted by fitting the obtained decay curves with exponential functions.

For investigation of the decay of highly charged ^{213}Fr, H-like ions, after they were produced and separated at the FRS, have been injected in the ESR at about 350 MeV/u. The
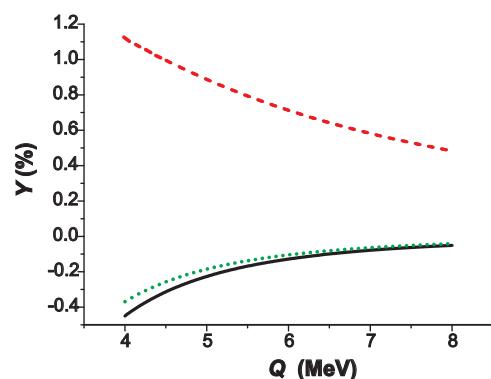
FIG. 6. Calculated relative change of the α decay rate in neutral atoms as compared to that of bare nuclei in the isotopes of Ra (full line) and Rn (dotted line), Y, against the released energy Q. Dashed curve is the same for Ra isotopes as calculated in the FS model.

TABLE II. Relative change of the decay rate Y between the decay in bare nuclei and He-like ions in the case of Ra isotopes.

A	Q_α (MeV)	$T_{1/2}$	$Y(\%)$
226	4.87063	1600 y	−0.246
224	5.78887	3.66 d	−0.14
222	6.681	38.0 s	−0.091
221	6.884	28 s	−0.083
220	7.595	18 ms	−0.060
214	7.273	2.46 s	−0.069
213	6.861	2.74 min	−0.084
212	7.0319	13.0 s	−0.071

decreasing number of parent ions has been observed by the Schottky techniques after each injection. Their identification was obtained by the Schottky mass spectrometry technique. Analyzing that experiment in the light of the present consideration, the following conclusions are worth noting.

First, the main idea of that experiment sounds striking: comparison of the lifetimes of neutral atoms with those in H-like ions. Why not just bare nuclei? One $1s$ electron already produces close to half the effect. Diminishing the effect by a factor of two requires adequately diminishing the experimental uncertainties, introducing unnecessary complications into an already difficult experiment.

Second, in order to investigate the presence of systematic errors in the ^{213}Fr half-life, a separate experiment has been performed at the LNS-INFN in Catania using a different implantation-decay setup and producing the ^{213}Fr ions by fusion-evaporation ^{11}B + ^{208}Pb reaction at 72 MeV. Finally, it was concluded that the half-life of neutral ^{213}Fr can be deduced with an accuracy of a few per thousand; in spite of that a large discrepancy (three σ) has been found in comparison with the literature value.

TABLE III. Relative change of the decay rate Y as in Table II calculated for other elements.

Nuclide	Q_α (MeV)	$T_{1/2}$	$Y(\%)$
^{221}Fr	6.4579	4.9 min	−0.10
^{220}Fr	6.8007	27.4 s	−0.086
^{213}Fr	6.9051	34.6 s	−0.082
^{220}Rn	6.40467	55.6 s	−0.10
^{219}Rn	6.9461	3.96 s	−0.080
^{212}Rn	6.385	23.9 min	−0.11
^{223}Ac	6.7831	2.10 min	−0.087
^{222}Ac	7.1374	5 s	−0.074
^{202}At	6.3537	184 s	−0.11
^{201}At	6.4733	89 s	−0.10
^{200}At	6.5964	43 s	−0.095
^{199}At	6.780	7.2 s	−0.087
^{198}At	6.893	4.2 s	−0.083
^{197}At	7.100	0.35 s	−0.075
^{196}At	7.200	0.3 s	−0.072
^{211}Po	7.5945	0.516 s	−0.061

In this respect, we note that our scheme will allow us to avoid systematic errors. In Ref. [31], separate measurements were made to reduce the statistical error: one at GSI and the other at the LNS-INFN. They compared the lifetimes in the H-like ions with those in neutral atoms, as measured by traditional techniques in stoppers. In the case of ^{213}Fr two independent neutral half-life measurements have been carried out, one at GSI and the other at the LNS-INFN, aimed at investigation of the presence of systematic errors in the neutral ^{213}Fr half-life. Record low statistical error of 2 per thousand was achieved in the both experiments. However, even though they agree, a discrepancy has been found with the value in the literature.

Our present proposal assumes that the both lifetimes—of the bare nuclei and He-like ions—will be measured in the same channel of the storage ring by the same Schottky method. Therefore, systematic uncertainties will be merely the same and mutually almost cancel one another in the relative half-life value of Y (3).

Third, the statistical uncertainty shown in the test experiment with H-like ions of ^{213}Fr was not yet enough for the present purposes, though the measured half-life $T_{1/2} = 34(6)$ s is compatible with the neutral half-life. In order to diminish the statistical uncertainty, one has to increase the measurement duration and also to increase the number of injected ions N. In our case of purely exponential decay, the statistical uncertainty of Y is $\approx 1/\sqrt{N}$. Regarding the latter dependence, one can target more long-lived isotopes in order to collect more ions for injection. Therefore, isotopes with the lifetimes ranging from minutes to even hours can be several times more effective for α decay measurements in ring experiments. Moreover, a typical Schottky measurement needs a period of several seconds. This will induce additional uncertainty in the case of radioactive nuclei. Making use of longer lived nuclides will also diminish this uncertainty. We think that such an experiment can be conducted with still higher efficiency at the new facility, by the super FRS Collaboration at the FAIR [32].

VI. CONCLUSION

We consecutively considered the effect of electron screening on the α decay rate from the viewpoint of its experimental investigation. The results presented previously demonstrate that within the adiabatic approach the effect of electron screening on the α decay rate is certainly negative, in spite of the attractive potential provided by the shell. The physics arguments in favor of this conclusion can be formulated as follows:

(i) Raising electron terms create resisting force acting from the shell on the α particle.

(ii) Experimentally observed drastic suppression of prompt fission in muonic atoms of actinide elements.

The main error of the FS model is in the identification of the inner electrostatic Coulomb potential, existing inside the parent atom, times $2e$ with the potential energy of the α particle in its motion through the electronic shell. Nonidentity of these concepts is demonstrated in the best way by addition of the constant into Eq. (7). Quint essence of the adiabatic approach is expressed by Eq. (15). This condition results in

the negative effect in the adiabatic approach and shows the reason for the positive effect obtained within the FS model. Flight of α particle through the electron shell rearranges the latter. In turn, this weakens the effect of the shell on the particle. Using the classic analogy, one can say that if the electrons are not fixed firmly on their places, then they take part of the momentum of the α particle and are partially carried by the particle. It is figuratively said in Ref. [10] that the α particle is accompanied with a tail of the atomic electrons when it crosses the shell. Such a loosed dynamics leads to softening of the electric field strength around the α particle in comparison with what is expected in the FS model.

General effect of retardation of the decay provided by the adiabatic approach is at the level of 10^{-3}. FS model results in the effect of the opposite sign and percent value. Its detection could be a difficult task. However, contemporary technique makes the observation of the effect and all the more testing for the difference between the models quite feasible. Moreover, speaking about experimental testing the models, this seems to be even more feasible, as one should choose between the estimates of different sign.

Moreover, application of the storage ring facilities makes use of any detectors unnecessary. The Schottky analysis allows one to conduct such an experiment. It needs no counters or other special techniques apart from the beams of the target nuclei or ions. Minutes or even seconds of the beam time may be enough for one experimental run. Such an impressive progress is provided by development of the experimental capabilities. Its astrophysical aspect fits perfectly into the research program of the FAIR project [32], and can be effectively performed, using the super FRS facility. Inferring the experimental results will certainly put a milestone on the way of astrophysical research of the processes occurring in the stellar plasma, including the Sun.

[1] E. E. Salpeter, Aust. J. Phys. **7**, 373 (1954).

[2] F. Belloni, Eur. Phys. J. A **52**, 32 (2016); N. Nissim, F. Belloni, S. Eliezer, D. Delle Side, and J. M. Martinez Val, Phys. Rev. C **94**, 014601 (2016).

[3] L. D. Blokhintsev and D. A. Savin, Phys. At. Nucl. **83**, 573 (2020).

[4] F. F. Karpeshin, Phys. Rev. C **87**, 054319 (2013).

[5] V. A. Erma, Phys. Rev. **105**, 1784 (1957).

[6] W. Rubinson and M. L. Perlman, Phys. Lett. B **40**, 352 (1972).

[7] K. U. Kettner, H. W. Becker, F. Strieder, and C. Rolfs, J. Phys. G: Nucl. Part. Phys. **32**, 489 (2006).

[8] N. T. Zinner, Nucl. Phys. A **781**, 81 (2007).

[9] Z. Patyk, H. Geissel, Y. A. Litvinov, A. Musumarra, and C. Nociforo, Phys. Rev. C **78**, 054317 (2008).

[10] F. F. Karpeshin and M. B. Trzhaskovskaya, Yad. Fiz. **78**, 1055 (2015) [Phys. At. Nucl. **78**, 993 (2015)].

[11] F. F. Karpeshin and M. B. Trzhaskovskaya, in *Exotic Nuclei, Proceedings of the First African Symposium. Cape Town, South Africa, 2–6 December 2013*, edited by E. Cherepanov *et al.* (World Scientific, New Jersey, 2014), p. 201.

[12] A. Y. Dzyublik, Phys. Rev. C **90**, 054619 (2014).

[13] N. Wan, C. Xu, and Z. Ren, Phys. Rev. C **92**, 024301 (2015).

[14] V. Y. Denisov and H. Ikezoe, Phys. Rev. C **72**, 064613 (2005).

[15] I. M. Band and M. B. Trzhaskovskaya, At. Data Nucl. Data Tables **35**, 1 (1986).

[16] R. P. Feynman, Phys. Rev. **56**, 340 (1939).

[17] I. M. Band, M. B. Trzhaskovskaya, C. W. Nestor Jr., P. O. Tikkanen, and S. Raman, At. Data Nucl. Data Tables **81**, 1 (2002); I. M. Band and M. B. Trzhaskovskaya, *ibid.* **55**, 43 (1993).

[18] G. C. Rodrigues *et al.*, At. Data Nucl. Data Tables **86**, 117 (2004).

[19] J. A. Wheeler, Rev. Mod. Phys. **21**, 133 (1949).

[20] D. F. Zaretski and V. M. Novikov, Nucl. Phys. **14**, 540 (1959).

[21] C. Rösel, P. David, H. Folger *et al.*, Z. Phys. A: Hadrons Nucl. **340**, 199 (1991).

[22] F. F. Karpeshin, *Prompt Fission in Muonic Atoms* (Nauka, St. Petersburg, 2006).

[23] M. Y. Balatz, L. N. Kondrat'ev, L. G. Landsberg, P. I. Lebedev, Y. V. Obukhov, and B. Pontecorvo, Zh. Eksp. Teor. Fiz. **38**, 1715 (1960) [Sov. Phys. JETP **11**, 1239 (1960)].

[24] G. E. Belovitskii, N. T. Kashchukeev, A. Mikhul, M. G. Petrashku, T. A. Romanova, and F. A. Tikhomirov, Zh. Eksp. Teor. Fiz. **38**, 404 (1960) [Sov. Phys. JETP **11**, 296 (1960)].

[25] D. F. Zaretski and V. M. Novikov, Nucl. Phys. **28**, 177 (1961).

[26] G. Leander and P. Möller, Phys. Lett. B **57**, 245 (1975).

[27] S. Ahmad, O. Häusser, J. A. Macdonald, B. H. Olaniyi, A. Olin, G. A. Beer, G. R. Mason, and S. N. Kaplan, Can. J. Phys. **64**, 665 (1986).

[28] F. Bosch, J. Phys. B: At. Mol. Opt. Phys. **36**, 585 (2003).

[29] R. B. Firestone, C. M. Baglin, and S. Y. F. Chu, *Table of Isotopes*, 8th ed. [CD-ROM] (Wiley-Interscience, New York, 1999).

[30] P. Kienle *et al.*, Phys. Lett. B **726**, 638 (2013).

[31] C. Nociforo *et al.*, Phys. Scr. T **150**, 014028 (2012).

[32] J. Äystö, K.-H. Behr, J. Benlliure *et al.*, Nucl. Instrum. Methods Phys. Res. B **376**, 111 (2016).